Systematic along-axis tidal triggering of microearthquakes observed at 9°50′N East Pacific Rise

D. F. Stroup,[1] M. Tolstoy,[1] T. J. Crone,[1] A. Malinverno,[1] D. R. Bohnenstiehl,[2] and F. Waldhauser[1]

Received 8 June 2009; revised 21 July 2009; accepted 23 July 2009; published 22 September 2009.

[1] Hydrothermal fluid circulation at mid-ocean ridges facilitates the exchange of heat and chemicals between the oceans and the solid Earth, and supports chemosynthetic microbial and macro-faunal communities. The structure and evolution of newly formed oceanic crust plays a dominant role in controlling the character and longevity of hydrothermal systems; however, direct measurements of subsurface processes remain technologically challenging to obtain. Previous studies have shown that tidally-induced stresses within the subseafloor modulate both fluid flow and microearthquake origin times. In this study, we observe systematic along-axis variations between peak microearthquake activity and maximum predicted tidal extension beneath the hydrothermal vent site at 9°50′N East Pacific Rise. We interpret this systematic triggering to result from pore-pressure perturbations propagating laterally through the hydrothermal system. Based on our observations and a one-dimensional pore pressure perturbation model, we estimate bulk permeability at $\sim 10^{-13}$ to 10^{-12} m^2 within layer 2B over a calculated diffusive lengthscale of 2.0 km. **Citation:** Stroup, D. F., M. Tolstoy, T. J. Crone, A. Malinverno, D. R. Bohnenstiehl, and F. Waldhauser (2009), Systematic along-axis tidal triggering of microearthquakes observed at 9°50′N East Pacific Rise, *Geophys. Res. Lett.*, *36*, L18302, doi:10.1029/2009GL039493.

1. Introduction

[2] Fluid flow within mid-ocean ridge hydrothermal systems is responsible for significant heat and solute fluxes between seawater and newly formed oceanic crust. The pattern, duration and intensity of hydrothermal circulation are strongly controlled by crustal permeability. Our best understanding of the permeability structure of these systems comes mainly from simple models of heat and fluid fluxes [e.g., *Lowell and Germanovich*, 1994; *Wilcock and McNabb*, 1996], yet despite decades of hydrothermal research, there are no direct observations of permeability on zero-age unsedimented crust. At mid-ocean ridges, tidal stresses can trigger earthquake activity [*Wilcock*, 2001; *Tolstoy et al.*, 2002; *Stroup et al.*, 2007]. These stresses also can generate pore pressure perturbations that modulate hydrothermal fluid flow rates and fluid exit temperatures [e.g., *Schultz and Elderfield*, 1997; *Glasby and Kasahara*, 2001; *Jupp and Schultz*, 2004; *Crone and Wilcock*, 2005]. In terrestrial settings, pore pressure perturbations associated with passing seismic waves may trigger earthquake activity [*Sturtevant et al.*, 1996; *Brodsky et al.*, 2000].

[3] In this study, we explore the spatial variability in the timing of microearthquakes recorded between October 2003 and April 2004 relative to the combined ocean and Earth tides at 9°50′N East Pacific Rise (EPR). The role of tidal stress variations in triggering microeathquakes during times of peak crustal extension has been previously proposed for this dataset [*Stroup et al.*, 2007]. At this site, solid Earth tidal stresses dominate earthquake triggering because of low amplitude ocean tides (typically <20 cm). Additionally, the high temperature hydrothermal vent field at 9°50′N EPR has been the focus of much interdisciplinary research since an eruption was discovered in 1991 [*Haymon et al.*, 1991]. In January 2006, after an increase in the seismic event rate over an ∼2.5 year period, the area erupted again repaving much of the ridge crest [*Tolstoy et al.*, 2006].

2. Microearthquakes at 9°50′N EPR

[4] From October 2003 to April 2004, seven ocean bottom seismographs (OBS) were deployed in a ∼4 km × 4 km array centered about the hydrothermal vent field at 9°50′N East Pacific Rise (EPR) [*Tolstoy et al.*, 2008] (Figure 1). Analyst-reviewed seismic phase arrivals and relative relocation techniques were used to generate a detailed catalog of nearly 10,000 microearthquakes (M_L < 2.0). Here we focus on a subset of 6,050 well-located earthquakes within the array, where bootstrap error analysis indicates a relative hypocentral accuracy of less than 50 m.

[5] During the seven-month monitoring period, seismic cracking is tightly constrained to the axial region, with most earthquakes occurring in the ∼500 m wide zone overlying the site's shallow (∼1.4 km depth) axial magma chamber (AMC) [*Kent et al.*, 1993]. The spatial pattern of small earthquakes suggests an along-axis pattern of hydrothermal flow [*Tolstoy et al.*, 2008], with cold seawater being entrained into the crust near ∼9°49.25′N and hot fluid exiting at a number of vent sites centered near ∼9°50.2′N (Figure 2). This along-axis flow is consistent with the expected alignment of cracks from vertical along-axis dikes, and with observations of ridge-parallel seismic anisotropy [e.g., *Burnett et al.*, 1989].

3. Microearthquakes and Tidal Phases

[6] Each microearthquake is assigned a tidal phase based on the combined predicted volumetric stresses induced by the solid Earth tide and the effects of ocean tidal loading. A

[1] Lamont-Doherty Earth Observatory, Earth Institute at Columbia University, Palisades, New York, USA.
[2] Department of Marine, Earth, and Atmospheric Sciences, North Carolina State University, Raleigh, North Carolina, USA.

0094-8276/09/2009GL039493

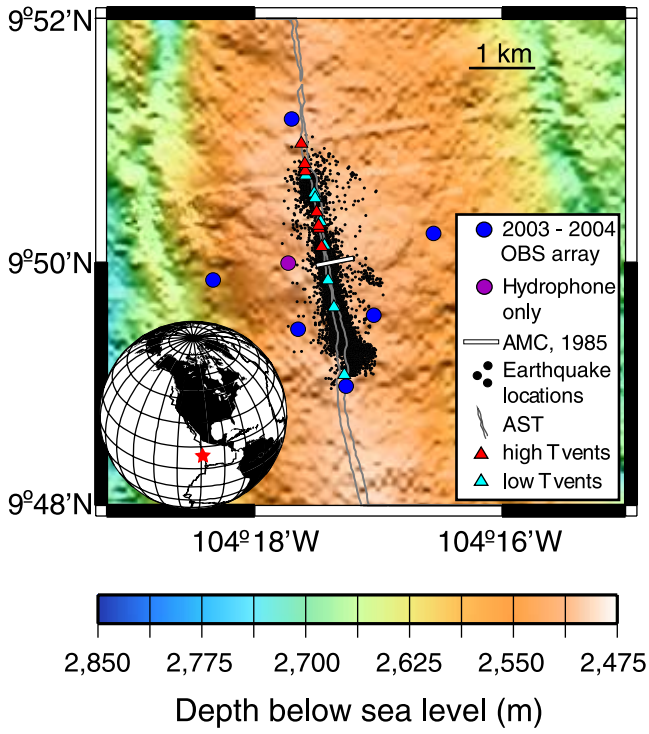

Figure 1. Bathymetric map with double-difference relocated epicenters [*Waldhauser and Ellsworth*, 2000] (black dots) located within the array of six OBSs (blue dots) and omni-directional hydrophone (purple dot). The high and low temperature vents (red and blue triangles, respectively), margins of the axial summit trough (grey lines) [*Fornari et al.*, 2004; *Soule et al.*, 2005], and the imaged AMC [*Kent et al.*, 1993] (white line) also are shown. The red star on the inset globe marks the location of 9°50′N East Pacific Rise. Modified from *Tolstoy et al.* [2008].

tidal phase of 0° represents maximum volumetric extension, while a tidal phase of ±180° represents maximum volumetric compression. Therefore, an earthquake that occurs halfway between high and low tides would be assigned a phase of 90°. Volumetric stress, an appropriate failure criterion for tensile or mixed-mode fracture of unknown orientation [*Bohnenstiehl and Carbotte*, 2001], is estimated using the GOTIC2 program [*Matsumoto et al.*, 2001], assuming a uniform crust composed of sheeted dikes (layer 2B; beneath ∼150 m depth on-axis [*Sohn et al.*, 2004]) with average P- and S-wave velocities of 4.5 km/s and 2.2 km/s [*Tolstoy et al.*, 2008], respectively, and an average density of 2,950 kg/m^3. On average, the combined Earth and ocean tide volumetric stress field exhibits a semi-diurnal periodicity, with peak predicted values of up to ±1.3 kPa, and reaches maximum extension ∼1 hour after peak ocean tidal height (Figure 1 of the auxiliary material)[1] [*Stroup et al.*, 2007]. However, we note that Earth tides may be significantly enhanced along the ridge-axis compared to model predictions [*Tolstoy et al.*, 1998], and these values should be viewed with that caveat in mind.

[7] Figure 2 shows the mean tidal phase of the microearthquakes mapped onto an along-axis cross-section, and Figure 3 shows the same data mapped onto a single along-axis dimension. The earthquakes within the inferred site of hydrothermal recharge at ∼9°49.25′N (downflow zone) and directly beneath the high temperature vents at ∼9°50.2′N (upflow zone) are triggered preceding or in phase with maximum predicted volumetric extension, while the earthquakes between these two zones (within the ∼500 m thick hydrothermal cracking zone directly above the AMC) are triggered after maximum predicted volumetric extension (Figures 2 and 3). To test the significance of these observations, we apply a Monte Carlo simulation [*Good*, 2005] to the events within the downflow and hydrothermal cracking zones, and find that the observed phase differences are statistically meaningful for this dataset (see discussion in Text S1).

4. One-Dimensional Poroelastic Model

[8] The along-axis temporal and spatial distribution of microearthquake triggering may reflect tidally-induced pore pressure perturbations traveling laterally away from the upflow and downflow zones into the hydrothermal cracking zone (Figures 2 and 3). The one-dimensional model for a semi-infinite half-space [*Fang et al.*, 1993] predicts a phase lag such as that observed on either side of the hydrothermal cracking zone (Figure 3) (see discussion in Text S2). Based on instrument coverage, we apply this model to the calculated mean phase angles of the best-constrained earthquakes from ∼9°49.35′N to ∼9°49.72′N (∼40% of the earthquake population – denoted by red error bars in Figure 3). The change in phase lag over this distance (∼685 m) allows for an estimation of the diffusive lengthscale that pore pressure perturbations can laterally propagate within the hydrothermal cracking zone. We weight the mean phase angles based on their 95% confidence intervals, and fit a least-squares regression line through the observed phase lag [*Menke*, 1984] (Figure 3). Based on this fit, we estimate the diffusive lengthscale to be ∼2.0 ± 0.47 km.

[9] This diffusive lengthscale is dependent on the fluid viscosity, formation permeability, and storage compressibility (see Text S2). To estimate the formation permeability, we determine the fluid viscosity using an equation of state for pure water as a function of temperature [*Holzbecher*, 1998]. We estimate the storage compressibility based on constant seismic velocities and rock density as above, on a rock bulk modulus for diabase of 70 GPa [*Pros et al.*, 1962], and on a drained frame bulk modulus, fluid bulk modulus and fluid density that vary as a function of porosity and temperature. To compute the fluid bulk modulus and fluid density, we use a combination of two equations of state [*Anderko and Pitzer*, 1993; *Pitzer et al.*, 1984] for 3.2 wt% NaCl-H_2O solution.

[10] Based on our model assumptions and a diffusive lengthscale of 2.0 km, we estimate bulk permeability within

[1]Auxiliary materials are available in the HTML. doi:10.1029/2009GL039493.

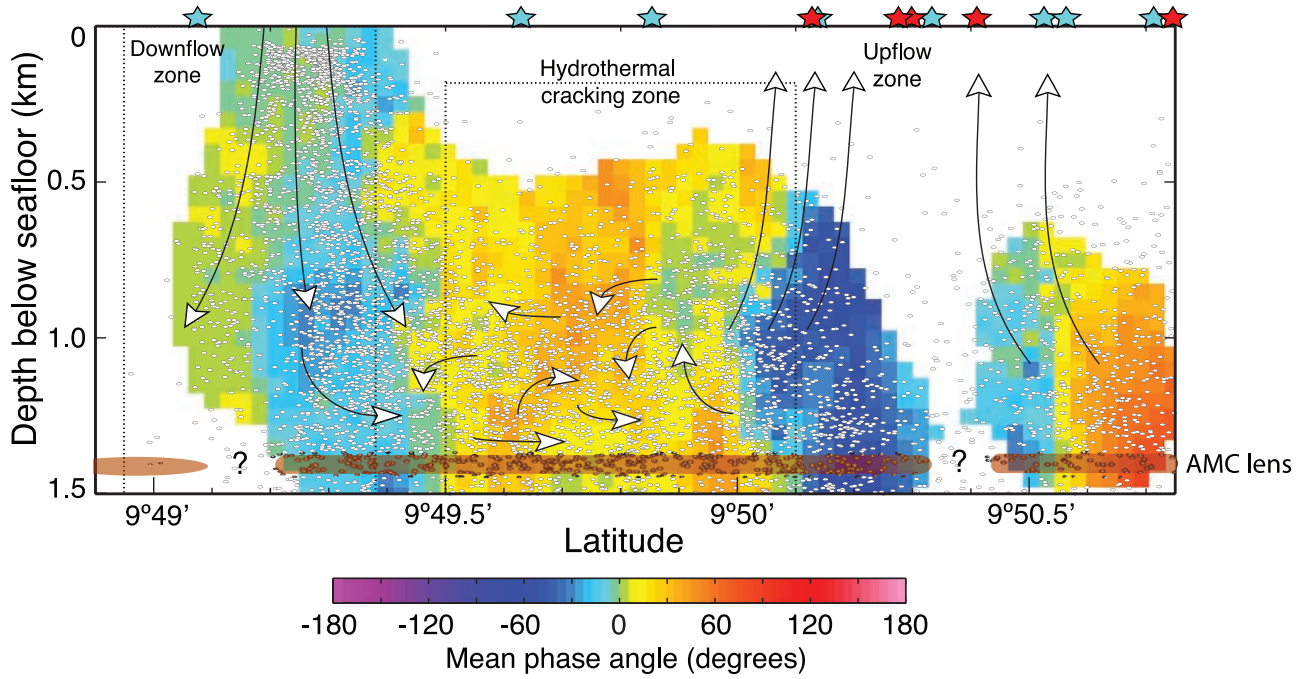

Figure 2. The color of each ~50 m × 50 m grid cell within the along-axis cross-section represents the mean phase angle of the closest 100 earthquakes using a 3D search radius. Regions with low data density (less than 100 earthquakes within a 175 m threshold) have been masked out. Arrows indicate the direction of inferred fluid flow through the hydrothermal cell, following interpretation by *Tolstoy et al.* [2008]. Statistical analysis was performed on the epicenters located within the downflow zone and hydrothermal cracking zone (black dashed boxes). The locations of high- and low-temperature vents (red and blue stars, respectively) also are shown.

the hydrothermal cracking zone at $\sim 1.75 \times 10^{-13}$ to $\sim 4.25 \times 10^{-12}$ m^2 for a range of temperatures (0–375°C) and porosities (2.5–5%) (Figure 4). The permeability range would be $\sim 3.63 \times 10^{-13}$ to 8.95×10^{-12} m^2 if we calculated the diffusive lengthscale for pore pressure perturbations traveling away from the upflow zone into the hydrothermal cracking zone.

5. Discussion

[11] Previous studies of tidal triggering at mid-ocean ridges have considered the instantaneous components of the tidal stresses only [*Wilcock*, 2001; *Tolstoy et al.*, 2002; *Stroup et al.*, 2007]; however, along-axis variability in the correlations between microearthquake activity and tidal phase at 9°50′N East Pacific Rise (Figures 2 and 3) suggest that a time-dependent component of pore pressure change may influence triggering in this system.

[12] In the presence of along-axis variations in the mechanical properties of the crust and pore fluid, tidally-induced stresses can generate horizontal pressure gradients [*Wang and Davis*, 1996]. The response of the hydrothermal system to tidal stresses will vary when the compressibility of the pore fluid or rock frame varies. Seawater entrained within the downflow zone is relatively cold and incompressible compared with fluids in the hydrothermal cracking zone, where heat is advected away from the axial magma chamber. Likewise, the rock frame within the downflow zone may be relatively compressible compared with the hydrothermal cracking zone due to enhanced stressing and cracking associated with the ~100 m offset in the ridge axis [e.g., *Wright et al.*, 1995].

[13] Tidal stresses can also generate horizontal pressure gradients in the presence of lateral permeability variations. Such along-axis permeability variations would change the depth to which seafloor pressure changes propagate into the crust, and therefore set up horizontal pressure gradients. Thus, the upflow and downflow zones may be regions of enhanced cracking and higher permeability surrounding a lower permeability hydrothermal cracking zone, where tidal triggering lags the effects of maximum predicted volumetric extension due to time-dependent horizontal pressure diffusion.

[14] We do not observe vertical pore pressure perturbations driving tidal triggering within our study region. At this site, the ocean tidal loading component is small and may be insignificant compared to horizontal pore pressure perturbations generated by the solid Earth tide. Another possibility may be that the skin depth across the center of the circulation cell lies above the hydrothermal cracking zone in a region where the background stress conditions do not promote earthquake activity. A relatively small increase in

permeability (approximately one order of magnitude) would extend this lengthscale beyond the depth of the seismically active hydrothermal cracking zone, such as that observed within the upflow and downflow zones.

[15] In conclusion, we use our observations of along-axis tidal triggering of microearthquakes to provide an *in situ* estimate of permeability at 9°50′N EPR. Our estimate of permeability is consistent with *in situ* measurements made at off-axis layer 2A (<300 m) boreholes ($\sim 10^{-15}$–10^{-12} m^2), and with on-axis numerical models that incorporate heat and fluid flow within the upper (<1500 m) oceanic basement ($\sim 10^{-16}$–10^{-9} m^2) [e.g., *Fisher*, 1998; *Lowell and Germanovich*, 1994; *Wilcock and McNabb*, 1996; *Wilcock and Fisher*, 2004; *Fisher et al.*, 2008].

[16] Our results support tidal forcing as a significant factor in mid-ocean ridge hydrothermal systems [e.g., *Schultz and Elderfield*, 1997; *Glasby and Kasahara*, 2001; *Jupp and Schultz*, 2004; *Crone and Wilcock*, 2005]. Fluid flow perturbations driven by the tides also may enhance subsurface mixing, which would have important implications for biological productivity [*Davis et al.*, 2000]. Our observations of along-axis trends in tidal triggering may allow for more sophisticated investigations into the heat and chemical exchange between the newly formed oceanic crust and hydrothermal fluids, and may provide insight into the plumbing supporting the subsurface biosphere.

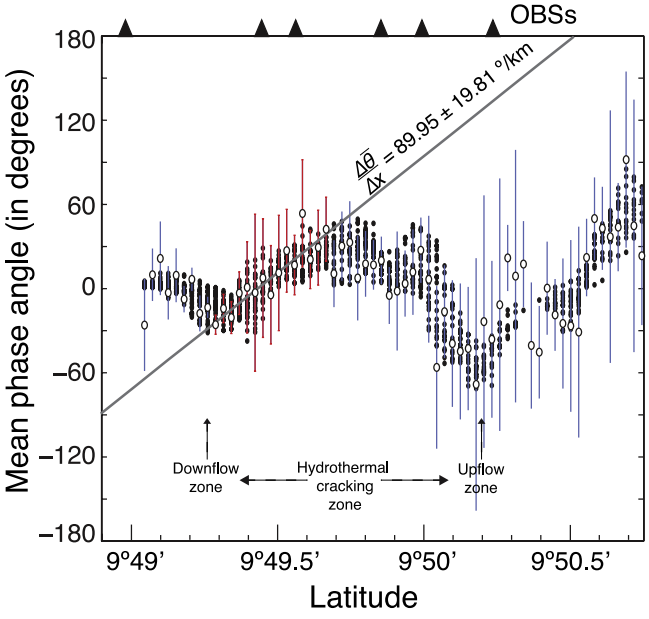

Figure 3. The mean phase angle from each of the nodes in Figure 2 shown as a function of latitude only (black dots). White circles show the mean phase angle of epicenters located within ∼50 m along-axis latitude bins, and the blue and red lines show their 95% confidence intervals. The weighted linear least-squares fit (black line) represents the lag in tidal triggering due to diffusive pore pressure perturbations traveling from the downflow zone into the hydrothermal cracking zone (delineations between these zones are approximate). Earthquakes within this region are best characterized due to the arrangement of OBSs (black triangles). A slope of ∼89.95 ± 19.81°/km gives a diffusive lengthscale of ∼2.0 ± 0.47 km.

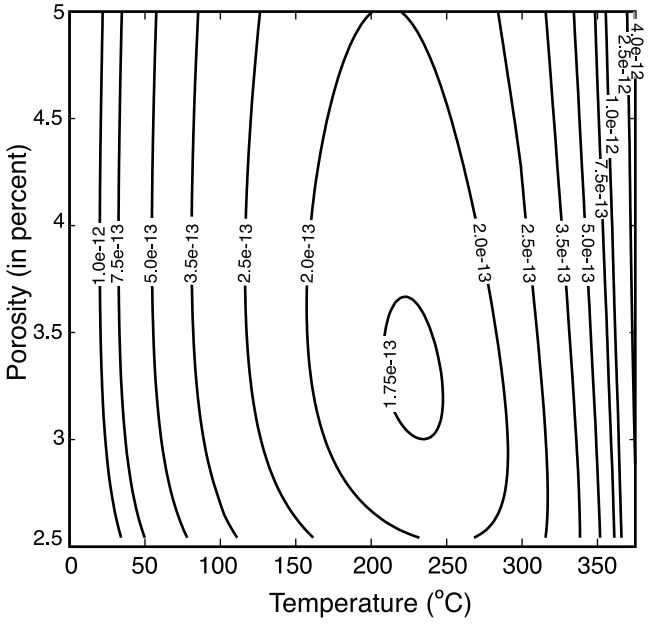

Figure 4. Permeability contours as a function of porosity and temperature. Permeability (in m^2) estimates (black lines) based on a 12.5 hour semi-diurnal tide and typical layer 2B properties. Permeability estimates range from $\sim 1.75 \times 10^{-13}$ to $\sim 4.25 \times 10^{-12}$ m^2. The contour intervals are not uniform for the sake of clarity.

[17] **Acknowledgments.** We thank Earl Davis, Robert Reves-Sohn, and William Wilcock for their constructive reviews of this manuscript. This work was supported by the National Science Foundation under grants OCE-0327283, OCE-0649538, and OCE-0732569.

References

Anderko, A., and K. S. Pitzer (1993), Equation of state representation of phase equilibria and volumetric properties of the system NaCl-H_2O above 573 K, *Geochim. Cosmochim. Acta*, *57*, 1657–1680, doi:10.1016/0016-7037(93)90105-6.

Bohnenstiehl, D. R., and S. M. Carbotte (2001), Faulting Patterns near 19°30′S on the East Pacific Rise: Fault formation and growth at a super-fast spreading center, *Geochem. Geophys. Geosyst.*, *2*(9), 1056, doi:10.1029/2001GC000156.

Brodsky, E. E., V. Karakostas, and H. Kanamori (2000), A New observation of dynamically triggered regional seismicity: Earthquakes in Greece following the August, 1999 Izmit, Turkey earthquake, *Geophys. Res. Lett.*, *27*, 2741–2744, doi:10.1029/2000GL011534.

Burnett, M. S., D. W. Caress, and J. A. Orcutt (1989), Tomographic image of the magma chamber at 12°50′N on the East Pacific Rise, *Nature*, *339*, 206–208, doi:10.1038/339206a0.

Crone, T. J., and W. S. D. Wilcock (2005), Modeling the effects of tidal loading on mid-ocean ridge hydrothermal systems, *Geochem. Geophys. Geosyst.*, *6*, Q07001, doi:10.1029/2004GC000905.

Davis, E. E., K. Wang, K. Becker, and R. E. Thomson (2000), Formation-scale hydraulic and mechanical properties of oceanic crust inferred from pore pressure response to periodic seafloor loading, *J. Geophys. Res.*, *105*, 13,423–13,435, doi:10.1029/2000JB900084.

Fang, W. W., M. G. Langseth, and P. J. Schultheiss (1993), Analysis and application of in situ pore pressure measurements in marine sediments, *J. Geophys. Res.*, *98*, 7921–7938, doi:10.1029/93JB00153.

Fisher, A. T. (1998), Permeability within basaltic oceanic crust, *Rev. Geophys.*, *36*, 143–182, doi:10.1029/97RG02916.

Fisher, A. T., E. E. Davis, and K. Becker (2008), Borehole-to-borehole hydrologic response across 2.4 km in the upper oceanic crust: Implications for crustal-scale properties, *J. Geophys. Res.*, *113*, B07106, doi:10.1029/2007JB005447.

Fornari, D. J., et al. (2004), Submarine lava flow emplacement at the East Pacific Rise 9°50′N: Implications for uppermost ocean crust stratigraphy and hydrothermal fluid circulation, in *Mid-Ocean Ridges: Hydrothermal Interactions Between the Lithosphere and Oceans*, *Geophys. Monogr. Ser.*, vol. 148, edited by C. R. German, J. Lin, and L. M. Parson, pp. 187–217, AGU, Washington, D. C.

Glasby, G. P., and J. Kasahara (2001), Influence of tidal effects on the periodicity of earthquake activity in diverse geological settings with particular emphasis on submarine hydrothermal systems, *Earth Sci. Rev.*, *52*, 261–297, doi:10.1016/S0012-8252(00)00031-3.

Good, P. I. (2005), *Permutation, Parametric, and Bootstrap Tests of Hypotheses*, 3rd ed., Springer, New York.

Haymon, R. M., D. J. Fornari, M. H. Edwards, S. Carbotte, D. Wright, and K. C. MacDonald (1991), Hydrothermal vent distribution along the East Pacific Rise crest (9°09′–54′N) and its relationship to magmatic and tectonic processes on fast-spreading mid-ocean ridges, *Earth Planet. Sci. Lett.*, *104*, 513–534, doi:10.1016/0012-821X(91)90226-8.

Holzbecher, E. O. (1998), *Modeling Density-Driven Flow in Porous Media*, Springer, New York.

Jupp, T. E., and A. Schultz (2004), A poroelastic model for the tidal modulation of seafloor hydrothermal systems, *J. Geophys. Res.*, *109*, B03105, doi:10.1029/2003JB002583.

Kent, G. M., A. J. Harding, and J. A. Orcutt (1993), Distribution of magma beneath the East Pacific Rise between the Clipperton Transform and the 9°17′N deval from forward modeling of common depth point data, *J. Geophys. Res.*, *98*, 13,971–13,995, doi:10.1029/93JB00706.

Lowell, R. P., and L. N. Germanovich (1994), On the temporal evolution of high-temperature hydrothermal systems at ocean ridge crests, *J. Geophys. Res.*, *99*, 565–575, doi:10.1029/93JB02568.

Matsumoto, K., T. Sato, T. Takenezawa, and M. Ooe (2001), GOTIC2: A program for computation of oceanic tidal loading effect, *J. Geod. Soc. Jpn.*, *47*, 243–248.

Menke, W. H. (1984), *Geophysical Data Analysis: Discrete Inverse Theory*, Academic, Orlando, Fla.

Pitzer, K. S., J. C. Peiper, and R. H. Busey (1984), Thermodynamic properties of aqueous sodium chloride solutions, *J. Phys. Chem. Ref. Data*, *13*, 1–106.

Pros, Z., J. Vaněk, and K. Klíma (1962), The velocity of elastic waves in diabase and greywacke under pressure up to 4 kilobars, *Stud. Geophys. Geod.*, *6*, 347–367, doi:10.1007/BF02585234.

Schultz, A., and H. Elderfield (1997), Controls on the physics and chemistry of seafloor hydrothermal circulation, *Philos. Trans. R. Soc., Ser. A*, *355*, 387–425, doi:10.1098/rsta.1997.0014.

Sohn, R. A., S. C. Webb, and J. A. Hildebrand (2004), Fine-scale seismic structure of the shallow volcanic crust on the East Pacific Rise at 9°50′N, *J. Geophys. Res.*, *109*, B12104, doi:10.1029/2004JB003152.

Soule, S. A., D. J. Fornari, M. R. Perfit, M. A. Tivey, W. I. Ridley, and H. Schouten (2005), Channelized lava flows at the East Pacific Rise crest, 9–10°N: The importance of off-axis lava transport in developing the architecture of young oceanic crust, *Geochem. Geophys. Geosyst.*, *6*, Q08005, doi:10.1029/2005GC000912.

Stroup, D. F., D. R. Bohnenstiehl, M. Tolstoy, F. Waldhauser, and R. T. Weekly (2007), Pulse of the seafloor: Tidal triggering of microearthquakes at 9°50′N East Pacific Rise, *Geophys. Res. Lett.*, *34*, L15301, doi:10.1029/2007GL030088.

Sturtevant, B., H. Kanamori, and E. E. Brodsky (1996), Seismic triggering by rectified diffusion in geothermal systems, *J. Geophys. Res.*, *101*, 25,269–25,282, doi:10.1029/96JB02654.

Tolstoy, M., S. Constable, J. A. Orcutt, H. Staudigel, and F. K. Wyatt (1998), Short and long baseline tiltmeter measurements on Axial Seamount, Juan De Fuca Ridge, *Phys. Earth Planet. Inter.*, *108*, 129–141, doi:10.1016/S0031-9201(98)00091-0.

Tolstoy, M., F. L. Vernon, J. A. Orcutt, and F. K. Wyatt (2002), The breathing of the seafloor: Tidal correlations of seismicity on Axial volcano, *Geology*, *30*, 503–506, doi:10.1130/0091-7613(2002)030<0503:BOTSTC>2.0.CO;2.

Tolstoy, M., et al. (2006), A seafloor spreading event captured by seismometers, *Science*, *314*, 1920–1922, doi:10.1126/science.1133950.

Tolstoy, M., F. Waldhauser, D. R. Bohnenstiehl, R. T. Weekly, and W.-Y. Kim (2008), Seismic identification of along-axis hydrothermal flow on the East Pacific Rise, *Nature*, *451*, 181–184, doi:10.1038/nature06424.

Waldhauser, F., and W. L. Ellsworth (2000), A double-difference earthquake location algorithm: Method and application to the northern Hayward fault, *Bull. Seismol. Soc. Am.*, *90*, 1353–1368, doi:10.1785/0120000006.

Wang, K., and E. E. Davis (1996), Theory for the propagation of tidally induced pore pressure variations in layered subseafloor formations, *J. Geophys. Res.*, *101*, 11,483–11,495, doi:10.1029/96JB00641.

Wilcock, W. (2001), Tidal triggering of microearthquakes on the Juan de Fuca Ridge, *Geophys. Res. Lett.*, *28*, 3999–4002, doi:10.1029/2001GL013370.

Wilcock, W. S. D., and A. T. Fisher (2004), Geophysical constraints on the sub-seafloor environment near mid-ocean ridges, in *The Subseafloor Biosphere at Mid-Ocean Ridges*, *Geophys. Monogr. Ser.*, vol. 144, edited by W. S. D. Wilcock et al., pp. 51–74, AGU, Washington, D. C.

Wilcock, W. S. D., and A. McNabb (1996), Estimates of crustal permeability on the Endeavour segment of the Juan de Fuca mid-ocean ridge, *Earth Planet. Sci. Lett.*, *138*, 83–91, doi:10.1016/0012-821X(95)00225-2.

Wright, D. J., R. M. Haymon, and K. C. Macdonald (1995), Breaking new ground: Estimates of crack depth along the axial zone of the East Pacific Rise (9°12′–54′N), *Earth Planet. Sci. Lett.*, *134*, 441–457, doi:10.1016/0012-821X(95)00081-M.

D. R. Bohnenstiehl, Department of Marine, Earth, and Atmospheric Sciences, North Carolina State University, Campus Box 8208, Raleigh, NC 27695-8208, USA.

T. J. Crone, A. Malinverno, D. F. Stroup, M. Tolstoy, and F. Waldhauser, Lamont-Doherty Earth Observatory, Earth Institute at Columbia University, 61 Route 9W, Palisades, NY 10964-8000, USA. (danielle@ldeo.columbia.edu)